Available online at www.sciencedirect.com
SCIENCE DIRECT®
European Journal of Mechanics B/Fluids 24 (2005) 642–658

Dam-break release of a gravity current in a stratified ambient

Marius Ungarish

Department of Computer Science, Technion, Haifa 32000, Israel

Received 24 November 2003; received in revised form 23 September 2004; accepted 24 February 2005

Available online 12 April 2005

Abstract

The 'dam-break' initial behaviour of an inviscid gravity current which is released from a lock and then propagates over a horizontal boundary at the base of a stratified ambient fluid is considered. Analytical and finite-difference solutions of the one-layer shallow-water equations are developed and compared for the linear stratification in a rectangular channel case, and corroborated by numerical solutions of the full two-dimensional Navier–Stokes equations. Extensions of the shallow-water solution to non-linear stratification, release from an elliptical reservoir, and axisymmetric geometry are also presented. The results indicate that the shallow-water formulation captures well the essential features of the motion, which are qualitatively similar to the non-stratified case, but with details modified by the stratification; in particular, the forward propagation of the head and the backward spread of the depression wave are reduced when the stratification increases.

Keywords: Gravity current; Stratified; Dam-break; Shallow-water; Finite-differences

1. Introduction

The dam-break flow of a water reservoir open to the atmosphere is a fundamental, well known and extensively researched problem in hydraulics, starting with Saint-Venant's solution in 1843, see for example Billingham and King [1]. A closely related fundamental problem appears in the study of the gravity current phenomena which are of interest in a wide range of industrial and geophysical application (Simpson [2], Huppert [3]). Indeed, the generation of a gravity current by the release of a stationary volume of fluid of given density from behind a lock into an ambient fluid of a (slightly) different density is a dam-break type problem in which the embedding fluid has some influence on the major motion of the released fluid. First, the 'reduced gravity' (based on the relative density difference) replaces the full gravitational acceleration of the classical water-air configuration; and second, the gravity current is subject to an additional condition, namely, that the front of the propagating fluid (i.e., the nose of the current) advances like a "wall" in the embedding fluid, see Klemp et al. [4]. An accepted versatile formulation of the gravity current flow is via the inviscid shallow-water (SW) approximation, and the dam-break problem provides elegant and insightful analytical solutions to these equations. This problem is therefore essential to the understanding of the initial motion of a gravity current and an efficient tool for testing numerical solvers of the SW equations. However, no analytical investigations of the dam-break problem for the gravity current in a stratified ambient have been presented, to our best knowledge. We think it is both of academic and practical importance to close this gap of knowledge concerning this fundamental problem.

Recent investigations of gravity currents in a (linearly) stratified ambient were presented by Maxworthy et al. [5] and by Ungarish and Huppert [6], hereafter referred to as UH. The former presented experimental measurements and numerical

E-mail address: unga@cs.technion.ac.il (M. Ungarish).

0997-7546/$ – see front matter
doi:10.1016/j.euromechflu.2005.02.001

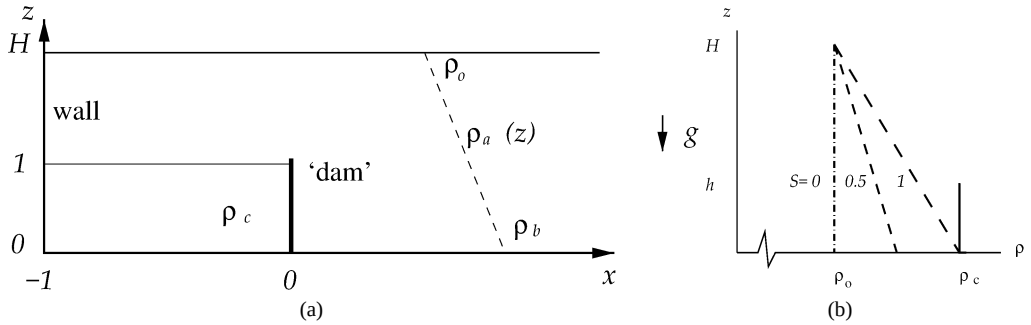

Fig. 1. Schematic description of the system at $t = 0$. (a) The geometry. Here the horizontal lengths are scaled with the length of the lock, x_0, and vertical lengths are scaled with the height of the lock, h_0. (In the elliptic lock system the dense fluid is initially in the domain $0 \leqslant z \leqslant (-x^2 - 2x)^{1/2}$, $-1 \leqslant x \leqslant 0$.) (b) Density profiles in the current (solid line) and ambient, for linear stratification at various values of S (dashed lines).

simulations. UH developed the one-layer SW equations and the nose boundary condition, and obtained solutions for the nose velocity, u_N, during the slumping phase of propagation with constant velocity. These theoretical results concerning the nose velocity are in very good agreement with the experiments of Maxworthy et al. [5], see Fig. 6 and Section 3 of UH. UH did not present SW solutions of the current, and therefore a logical step to advance the previous theoretical-analytical work is the investigation of the dam-break problem. This study requires a detailed solution of the SW equations during a significant time interval following the release from behind the lock, for which the previously calculated u_N will serve as a reliable boundary condition. The analysis is expected to provide insights into the modeling and understanding of the time-dependent constant-volume gravity current (or intrusion) in a stratified ambient. We notice that, to our best knowledge, no reliable theoretical predictive tools are available for the analysis of this phenomenon, and we think it would be beneficial to close the gap with the non-stratified well developed counterpart.

These considerations motivated the present work, whose combined objectives are (a) to extend the dam-break problem to a gravity current in a stratified ambient, and (b) to extend the study of UH to the initial motion of the entire gravity current via the solution of the SW equations, and also to non-linear stratifications.

The system under consideration is sketched in Fig. 1: a layer of ambient fluid of height H and (stable) density $\rho_a(z)$, lies above the horizontal surface $z = 0$. Gravity acts in the $-z$ direction. In the rectangular case considered here the system is bounded by parallel vertical smooth impermeable surfaces and the current propagates in the direction labeled x. A given volume of homogeneous fluid of density $\rho_c \geqslant \rho_a(z = 0) \equiv \rho_b$ and kinematic viscosity ν, is initially at rest in a rectangular box of height h_0 and length x_0, bounded by a 'dam' (or gate) at $x = 0$ and a solid wall at $x = -x_0$. We assume that the height of the dense fluid does not exceed that of the ambient. At time $t = 0$ the dam is instantaneously removed, and a two-dimensional current commences to spread. We assume that the Reynolds number of the horizontal flow, *Re*, defined below, is large and hence viscous effects can be neglected. We attempt to predict the shape (position of nose and upper interface) of the dense fluid (current) and the main (horizontal) velocity field within.

The structure of the paper is as follows. In Section 2 the shallow-water equations of motion and the appropriate boundary conditions are developed. Analytical and finite-difference solutions for the dam-break stage are presented in Section 3, for linear and non-linear stratifications. Some numerical results of the Navier–Stokes equations are also presented for corroboration of the SW predictions. The release from the classical rectangular reservoir is briefly contrasted with release from an elliptical container. In Section 4 concluding remarks are given. The non-stratified counterpart results are summarized in Appendix A, and a brief extension to the axisymmetric configuration is provided in Appendix B.

2. Formulation and shallow-water (SW) approximation

The configuration is sketched in Figs. 1 and 2. We use a $\{x, y, z\}$ Cartesian coordinate system with corresponding $\{u, v, w\}$ velocity components, and assume that the flow does not depend on the coordinate y and that $v \equiv 0$. Initially, the height of the released current is h_0, its length is x_0 and the density is ρ_c. The height of the ambient fluid is H and the density in this domain decreases with z from ρ_b to ρ_o. (The subscripts b, o refer to bottom and open surface values.)

It is convenient to use ρ_o as the reference density and to introduce the reduced density differences

$$\epsilon = \frac{\rho_c - \rho_o}{\rho_o}, \qquad \epsilon_b = \frac{\rho_b - \rho_o}{\rho_o}, \tag{2.1}$$

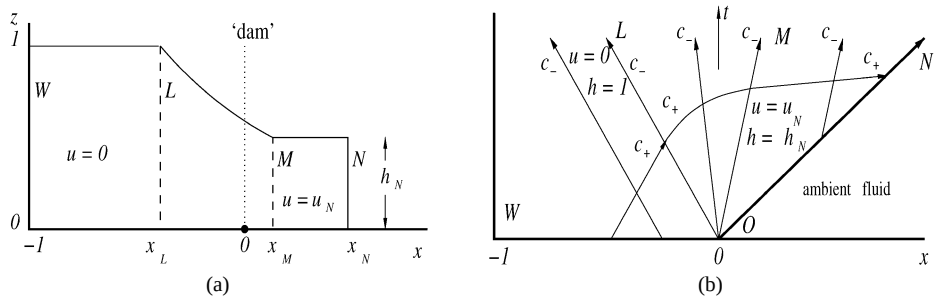

Fig. 2. Schematic description of the current during the initial dam-break stage. (a) Geometry in xz plane; (b) characteristics in xt plane (here point O is the origin).

and

$$S = \frac{\epsilon_b}{\epsilon}, \tag{2.2}$$

from which it follows that

$$\rho_c = \rho_o(1+\epsilon), \qquad \rho_a(z) = \rho_o\big[1+\epsilon S\sigma(z)\big], \tag{2.3}$$

where $\sigma(z)$ represents the form (shape) of stratification, a continuous and typically decreasing (allowing for some piecewise constant regions) function of $z \in [0, H]$, subject to

$$\sigma(0) = 1, \qquad \sigma(H) = 0. \tag{2.4}$$

The most common case is the linear stratification,

$$\sigma_{\text{linear}}(z) = 1 - \frac{z}{H}. \tag{2.5}$$

We shall consider only $0 \leqslant S \leqslant 1$. The classical homogeneous ambient case is recovered by setting $S = 0$. We also define the reference reduced gravity,

$$g' = \epsilon g, \tag{2.6}$$

where g is the gravitational acceleration. The buoyancy frequency is given by $\mathcal{N}^2 = -g'S(\mathrm{d}\sigma/\mathrm{d}z)$, and, for the linear case, $\mathcal{N}^2 = g'S/H$.

Following UH, we use a one-layer approximation which is expected to capture many of the important features of the flow, although it discards the internal waves in the ambient, as discussed in Section 2.3. This is the simplest shallow-water model, and therefore provides a convenient (perhaps even necessary) idealization for the analytical discussion of the dam-break stage. The dense fluid is separated from the ambient fluid by a sharp interface $z = h(x,t)$, $-x_0 \leqslant x \leqslant x_N(t)$, where $x_N(t)$ is the position of the vertical nose, assumed a shock discontinuity. The subscript N denotes the nose of the current. We assume that in the ambient fluid domain $u = v = w = 0$ and hence the fluid is in purely hydrostatic balance and maintains the initial density $\rho_a(z)$. The motion is assumed to take place in the lower layer of dense fluid only, $-x_0 \leqslant x \leqslant x_N(t)$ and $0 \leqslant z \leqslant h(x,t)$. Here the motion is governed by the balance between pressure and inertia forces in the horizontal direction. We assume $\epsilon \ll 1$ and employ the Boussinesq approximation.

In the motionless ambient fluid, which is open to the atmosphere, the pressure does not depend on x, and the hydrostatic balances $\partial p_i/\partial z = -\rho_i g$, where $i = a$ or c, and use of (2.3) yield

$$p_a(z,t) = -\rho_o\left[z + \epsilon S\int_0^z \sigma(z')\,\mathrm{d}z'\right]g + C, \tag{2.7}$$

$$p_c(x,z,t) = -\rho_o(1+\epsilon)gz + f(x,t). \tag{2.8}$$

Pressure continuity at the interface $z = h(x,t)$ determines the function $f(x,t)$ of (2.8) and we obtain, after some algebra,

$$p_c(x,z,t) = -\rho_o(1+\epsilon)gz + \rho_o g'\left[h(x,t) - S\int_0^{h(x,t)} \sigma(z')\,\mathrm{d}z'\right] + C, \tag{2.9}$$

and consequently

$$\frac{\partial p_c}{\partial x} = \rho_o g'\frac{\partial h}{\partial x}\big[1 - S\sigma(h)\big]. \tag{2.10}$$

2.1. Governing SW equations

It is convenient to scale the dimensional variables (denoted here by asterisks) as follows

$$\{x^*, z^*, h^*, H^*, t^*, u^*, p^*\} = \{x_0 x, h_0 z, h_0 h, h_0 H, T t, U u, \rho_o U^2 p\}, \tag{2.11}$$

where

$$U = (h_0 g')^{1/2} \quad \text{and} \quad T = x_0/U. \tag{2.12}$$

Here h_0 and x_0 are the initial height and length of the current, U is a typical inertial velocity of propagation of the nose of the current and T is a typical time period for longitudinal propagation over a typical distance x_0. These scalings are convenient for comparisons with previous papers on both stratified and homogeneous cases.

Hereafter, dimensionless variables will be used. In our configurations $H \geqslant 1$.

We employ the inviscid Boussinesq fluid simplifications, under the assumptions that the typical Reynolds number, $Re = Uh_0/\nu$, is large, and the relative density difference, ϵ, is small. The z-average of the horizontal momentum equation, on account of (2.10), and in conjunction with volume continuity, produces a system of equations for the height of the interface, $h(x,t)$, and for the averaged longitudinal velocity, $u(x,t)$. In characteristic form these simplified continuity and momentum equations are

$$\begin{bmatrix} h_t \\ u_t \end{bmatrix} + \begin{bmatrix} u & h \\ 1 - S\sigma(h) & u \end{bmatrix} \begin{bmatrix} h_x \\ u_x \end{bmatrix} = \begin{bmatrix} 0 \\ 0 \end{bmatrix}. \tag{2.13}$$

2.2. Characteristics and boundary conditions

For the stratification assumed in this study the coefficient matrix of (2.13) has real eigenvalues and a full set of eigenvectors, and hence the system (2.13) is hyperbolic, like in the homogeneous $S = 0$ classical case.

Following the standard procedure, we obtain the characteristic speeds of propagation,

$$c_\pm = u \pm \left[h\big(1 - S\sigma(h)\big)\right]^{1/2}, \tag{2.14}$$

and the relationships between the variables on the trajectories with $\mathrm{d}x/\mathrm{d}t = c_\pm$,

$$\left[\frac{1 - S\sigma(h)}{h}\right]^{1/2} \mathrm{d}h \pm \mathrm{d}u = 0. \tag{2.15}$$

The initial conditions for the dam-break problem are: zero velocity and unit dimensionless height and length at $t = 0$. The boundary conditions are: the velocity at $x = -1$ is zero, and an additional condition for the velocity u is needed at the nose $x = x_N(t)$.

In the classical hydraulic dam-break problem the nose height of the water (that propagates against the negligible resistance of the embedding air) decreases smoothly to zero at $x_N(t)$, and hence the nose velocity follows straightforwardly from the internal solution, see Appendix A. For the gravity current case the nose, that encounters the resistance of the quite dense embedding fluid, is a discontinuity, and the proper boundary condition for the velocity at the nose is essential for a proper physical definition and mathematical closure of the problem, see Klemp et al. [4]. The consensus developed for the homogeneous ambient case is that the nose of a realistic space- and time-dependent gravity current obeys a local quasi-steady correlation at $x = x_N(t)$ between the height h_N and velocity u_N, whose essentials are provided by the idealized balance of flow forces and volume continuity discussed by Benjamin [7].

UH argued that, like in the homogeneous ambient case, the velocity of the nose is proportional to the square-root of the pressure head (per unit mass), and, moreover, that the factor of proportionality, defined as the Froude number, Fr, is provided by the same correlation as in the homogeneous gravity current. These arguments are supported by the good agreement between the calculated u_N and the experimental values of Maxworthy et al. [5]. We argue that these connections remain valid for a more general stable stratification, as considered here. The needed pressure head is given by $p_c - p_a$ at $z = 0$ and $x = x_N$, see (2.7) and (2.9), scaled with $g'h_0$. The resulting nose velocity can be expressed as

$$u_N = Fr(h_N) h_N^{1/2} \times \left[1 - S\Lambda(h_N)\right]^{1/2}, \tag{2.16}$$

where

$$\Lambda(h_N) = \frac{1}{h_N} \int_0^{h_N} \sigma(z)\,\mathrm{d}z, \tag{2.17}$$

and, in the particular linear stratification case, by (2.5) we obtain

$$\Lambda(h_N) = \Lambda_{\text{linear}}(h_N) = 1 - \frac{1}{2}\frac{h_N}{H}. \tag{2.18}$$

The term in the square brackets of (2.16) is smaller than 1 for $S > 0$, and expresses the explicit reduction of the driving pressure force on the head due to the stratification effects.

The value of Fr, which is needed to close the formulation, is provided by the semi-empirical correlation derived by Huppet and Simpson [8]

$$Fr = \begin{cases} 1.19 & (0 \leqslant h_N/H \leqslant 0.075), \\ 0.5H^{1/3}h_N^{-1/3} & (0.075 \leqslant h_N/H \leqslant 1). \end{cases} \tag{2.19}$$

Use of this correlation in this analysis is justified by (a) its extensive use in various non-stratified predictions, and hence we are able to straightforwardly recover this case for $S = 0$, and (b) the good agreement (typically within 5%) of the SW velocity of propagation, u_N, with laboratory and numerical experiments reported by UH (see Fig. 6 and Sections 3 and 4 there). These agreements were obtained, without any adjustable parameter, over a wide range of the parameters S and H (one can argue that (2.19) contains an experimental adjustment, but this has not been introduced by UH). We emphasize that the subsequent analysis of the dam-break flow is not affected by the exact form of the closure correlation (except for some minor numerical details) and hence the conclusion remain valid for a more general $Fr(h_N)$.

2.3. Discussion

The foregoing closed formulation of the one-layer SW model for a quite general stratification is a versatile tool. It can be easily extended to dam-break release from non-rectangular reservoirs, see Section 3.3, and axisymmetric configurations (Appendix B). Moreover, this formulation is also effective in the investigation of intrusions (see [9]) and formation of lenses in rotating systems (see [10]). The stratification enters the model by two effects: (a) the pressure gradient in the momentum equation is reduced as S increases (this also affects the velocity and balances on the characteristics); and (b) the velocity of the nose is reduced as S increases. The simplifying assumptions introduced during the derivation of the model are expected to impose restrictions on the range of applicability and accuracy of the model. These limitations cannot be firmly assessed at this stage, but we rather expect that they will be inferred eventually by the interpretation of the results and comparison with numerical and laboratory experiments (if and when available).

The assumption of unperturbed $\rho_a(z)$ above and in front of the current gives rise to concerns, as follows. First, in real configurations some density perturbations are expected because of the presence of internal gravity waves. The velocity of the leading linear waves in the unperturbed fluid (Baines [11]) is, in the present scaling,

$$u_w = \pm\frac{1}{\pi}\sqrt{SH} \tag{2.20}$$

and a gravity current may be subcritical, $u_N < u_w$, or supercritical, $u_N > u_w$, during the initial slumping stage (depending on H and S). One may therefore argue that the effect of the waves is insignificant for supercritical currents; this is consistent with experimental observations. Moreover, there is experimental evidence that even in the subcritical case the waves start to influence the motion only after a significant distance of propagation (see [5], Fig. 6), which we can estimate as follows. In analogy with the "small amplitude topography" analysis of Baines ([11], Section 5.2), we can consider the dense fluid current as an obstacle at the bottom of a moving bulk of stratified fluid. Hence the typical wave-length of the perturbation in the ambient, scaled with x_0, is $\lambda = 2\pi(H/S)^{1/2}(h_0/x_0)u_N$ (consistent with the observation of [5] Fig. 14 for the subcritical regime). The inherent time-dependent shape of the current during the relatively short slumping phase renders the steady-state features of the classical investigations of the stratified flow over a fixed obstacle, and in particular Long's model results, irrelevant to the present problem. We use instead the empirical observation of [5] about waves that develop during the initial propagation. The first wave is initially locked to the head, but after a while a second wave is generated, and next a relative motion begins between the head and first wave. The head moves with the original velocity, u_N, during the formation of the first and second wave, and for the additional period of time required for the trough of the first wave to catch up the nose. This observation leads to the estimate that in subcritical currents the distance of propagation before the first head-wave interaction occurs is $4\pi(H/S)^{1/2}(h_0/x_0)u_N$, approximately (i.e., two wave-lengths; this estimate is consistent with the experiments of [5]). The conclusion is that a well defined initial slumping motion with constant velocity over a significant distance is expected for both sub- and super-critical currents, with little influence from the internal gravity waves. Second, the streamline of the moving head is expected to elevate the encountered isopycnals to $z \approx h_N$. This local modification of the density is expected to make a minor contribution to the global relevant pressure balances, at least for a deep ambient configuration, $H \gg 1$.

The nose condition assumption (2.16) can be firmly justified only in the $S = 0$ limit, on account of the theoretical steady-state analysis of Benjamin [7], and various subsequent tests and modifications, as discussed by Rottman and Simpson [12], Huppert

and Simpson [8], Klemp et al. [4] and Ungarish and Zemach [13]. A theoretical result similar to Benjamin's can be derived for the more general $S > 0$ case, e.g. via the solution of Long's steady-state inviscid model, but this complex task is beyond the scope of the present investigation, and in any case the relevance of this solution to the propagation of a time-dependent current is not obvious (see Baines [11]). The initial-value and the steady-state results of gravity current problems cannot be straightforwardly matched; typical difficulties of "reconciliation" between the corresponding formulations are discussed by Klemp et al. [4]. It turns out that some trial-and-error is necessary, and in this spirit we employ (2.16), because: (a) This is a plausible closure formula, based on valid physical arguments, that involves the necessary dimensionless parameters, and can be easily replaced in the methodology of solution with other formulas when available. (b) This closure provided very good agreements with experiments for the initial slumping velocity u_N, for a wide range of S and H, as detailed in UH. Such agreement cannot be a coincidence, and hence we are confident that this formula captures correctly the correlation between the involved variables. We expect that the dedicated theoretical studies of the steady-state nose motion will end up with a result that supports our formula, otherwise it will be difficult to bring them into accord with available measurements.[1]

Thus, in spite of imperfect assumptions and possible formal restrictions on the range of applicability, we think that this SW theory is an acceptable starting point for the solution of the time-dependent gravity current. Criticism and improvements are expected to develop in the process of solution and application in various circumstances. We must keep in mind that our reference for performances must be the corresponding non-stratified one-layer SW model. We shall see that, in spite the aforementioned concerns and restrictions contributed by the stratification of the ambient, the overall predictive powers of the classical $S = 0$ one-layer SW approximation are quite straightforwardly extended to the stratified ambient case, for the time intervals relevant to the dam-break problem, at least.

3. Solutions

The numerical solution of the SW equations was performed by a finite-difference Lax–Wendroff scheme [14,15]. This method has been used successfully for non-stratified ($S = 0$) gravity currents in various circumstances (Bonnecaze et al. [16], Ungarish and Huppert [17]) and here the necessary modifications of the equations for $0 < S \leqslant 1$ and boundary conditions were made. The domain $-1 \leqslant x \leqslant x_N(t)$ was mapped into $0 \leqslant y \leqslant 1$, and the latter discretized into equidistant intervals. In this work we used a grid with 200 intervals and time step 1/200. The results will be presented later.

Of particular interest to the present study are the analytical features of the solution, derived by the method of characteristics. The typical expected behaviour that guides the analysis is presented in Fig. 2, in the physical plane xz and in the characteristic plane xt. Point W represents the fixed position of the wall ($x = -1$). Points L and M represent the moving loci of the end of the unperturbed domain and start of nose-dominated domain. The interface $h(x, t)$ is inclined in the LM domain. The letter N represents the moving nose. Point O is the origin $x = 0, t = 0$ in the characteristic plane. We remark that M is not necessarily to the right of the origin as sketched in Fig. 2.

Considering (2.15) we define

$$\Upsilon(h) = \int_0^h \left[\frac{1 - S\sigma(h')}{h'}\right]^{1/2} \mathrm{d}h', \tag{3.1}$$

and consequently the balance on the characteristics (2.15) can be integrated to yield

$$u + \Upsilon(h) = \Gamma_+, \tag{3.2}$$

$$u - \Upsilon(h) = \Gamma_- \tag{3.3}$$

for the trajectories $\mathrm{d}x/\mathrm{d}t = c_\pm$, see (2.14), on which $\Gamma_\pm$ are constants.

The WOL characteristic region is covered by characteristics that start at $t = 0$ in the domain $x < 0$ and carry the information $u = 0$ and $h = 1$, i.e., $\Gamma_+ = -\Gamma_- = \Upsilon(1)$. Substitution of these conditions in (3.2), (3.3) yields $u = 0$ and $h = 1$ in the entire WOL domain. The characteristics that carry these values are straight lines, and the largest x of the pertinent domain is given by the line OL:

$$x_L(t) = c_- t = -\left[1 - S\sigma(1)\right]^{1/2} t. \tag{3.4}$$

We conclude that the stratification decreases the speed of backward propagation of position L. The result (3.4) is valid for $t \leqslant [1 - S\sigma(1)]^{-1/2}$, until L reaches the wall at $x = -1$. This occurrence can be considered the end of the dam-break stage.

[1] We may recall that in the $S = 0$ case Benjamin's rigorous result was preceded by a similar formula derived about 30 years earlier by von Kármán from simplified arguments.

Consider the solution of (3.2), (3.3) in the LOM domain of characteristics. Assume that c_+ characteristics from the above mentioned WOL domain enter the present domain, i.e., on c_+

$$u + \Upsilon(h) = \Upsilon(1), \tag{3.5}$$

while the c_- characteristics are emanated from point O as a fan with various initial h, i.e.,

$$u - \Upsilon(h) = \Gamma_- \quad (h_N \leqslant h \leqslant 1) \tag{3.6}$$

on

$$\frac{\mathrm{d}x}{\mathrm{d}t} = c_- = u - \left[h(1 - S\sigma(h)\right]^{1/2}, \quad x(0) = 0. \tag{3.7}$$

The intersection of (3.5) and (3.6), and use of (3.7) yield, again,

$$u = \Upsilon(1) - \Upsilon(h) = \text{const} \tag{3.8}$$

and $h = \text{const}$ on the ray

$$\frac{x}{t} = u - \left[h\big(1 - S\sigma(h)\big)\right]^{1/2}. \tag{3.9}$$

If (x/t) is a monotonic decreasing function of h, the line OM is given by (3.8) and (3.9) with $h = h_N$.

Finally, the abovementioned c_+ characteristics are expected to enter the characteristic region MON where $u = u_N$ and $h = h_N$. The intersection of (3.8) with (2.16),

$$u_N = \Upsilon(1) - \Upsilon(h_N) = Fr(h_N)h_N^{1/2} \times \left[1 - S\Lambda(h_N)\right]^{1/2}, \tag{3.10}$$

provides the value of h_N. The c_- characteristics in the MON domain are lines parallel to OM and carry the consistent information $u = u_N$, $h = h_N$.

The essential dependency of h and u in the characteristic domain LOM is on (x/t), i.e., it contains the similarity of the classical problem. Thus, the scaling length x_0 can be chosen arbitrary to describe the motion until L encounters the back wall.

An inspection of the results shows that for the quite general stable stratification $\sigma(z)$ assumed here, both velocities c_- and u are monotonic functions of h in the characteristic domain LOM; actually, both c_- and u increase as h decreases from 1 to h_N. At all positions of interest the c_+ velocity is larger than u. This confirms the assumption that the domain of the gravity current is covered by the considered characteristics. Also, this proves that no discontinuities of h or u develop in the solution of $0 < S \leqslant 1$ cases, similar to the classical $S = 0$ case.

Indeed, for $S = 0$ the classical non-stratified dam-break solution is immediately recovered from (3.1)–(3.10), see Appendix A. There are, however, interesting differences in the details of the motion between the $S = 0$ and $S > 0$ cases. In general, for $S > 0$ the solution in the characteristic domains LOM and MON requires numerical evaluation of $\Upsilon(h)$ and $\Lambda(h_N)$, but analytical results can be derived for the *linear* case, see (2.5), to which we now proceed.

3.1. Linear stratification, $\sigma(z) = 1 - z/H$

Consider $S = 1$. In this case (3.1) and (3.8) yield

$$\Upsilon(h) = \frac{1}{\sqrt{H}}h, \quad u = \frac{1}{\sqrt{H}}(1 - h) \quad (0 \leqslant h \leqslant h_N) \tag{3.11}$$

whose substitution in (3.9) and arrangement give

$$h = \frac{1}{2}\left(1 - \sqrt{H}\,\frac{x}{t}\right), \quad u = \frac{1}{2}\left(\frac{1}{\sqrt{H}} + \frac{x}{t}\right), \quad -\frac{1}{\sqrt{H}} \leqslant x/t \leqslant \frac{1}{\sqrt{H}}(1 - 2h_N) \tag{3.12}$$

in the region LOM.

The value of h_N is provided by (3.10) and (2.18)

$$u_N = \frac{1}{\sqrt{H}}(1 - h_N) = Fr(h_N)\frac{h_N}{\sqrt{2H}}, \tag{3.13}$$

and the results are plotted in Fig. 3. In particular, for $H > 7.4$, $Fr = 1.19$ and (3.13) gives $h_N = 0.543$. The same equation and results for h_N and u_N have been obtained by UH without solving the details of the region behind the nose.

A typical comparison between the analytical and numerical dam-break results is shown in Fig. 4. The agreement is, as expected, excellent, which provides a straightforward verification of both solutions. The remarkable features for the linear stratification with $S = 1$ are (a) the profile of h vs x in the LM domain is linear, in contrast to the parabolic shape in the

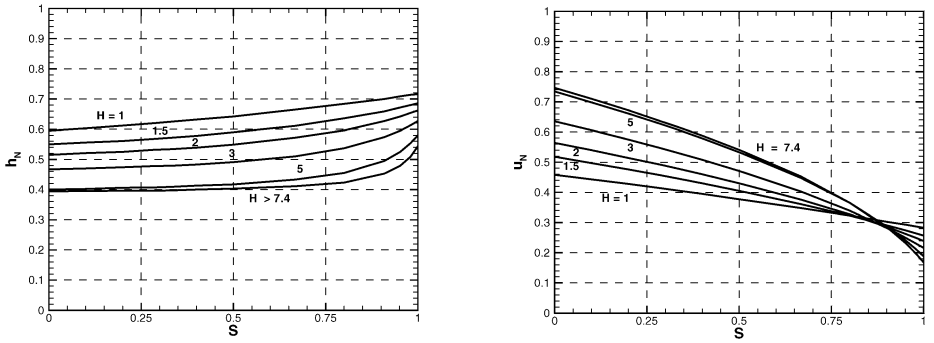

Fig. 3. Linear stratification, h_N and u_N as a function of S for various H.

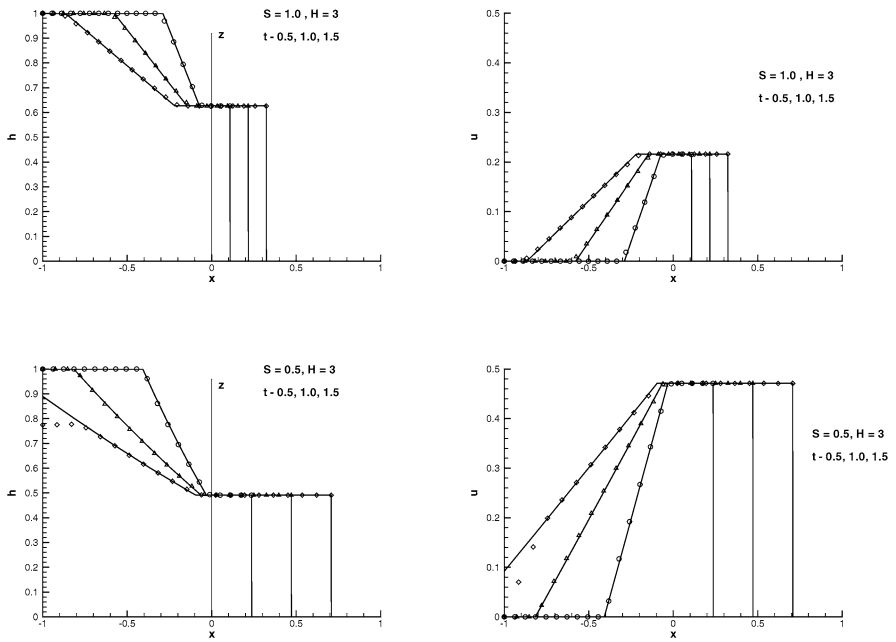

Fig. 4. Analytical (lines) and SW numerical (symbols) results, of $h(x)$ and $u(x)$ at $t = 0.5, 1.0, 1.5$, for linear stratification and $H = 3$. $S = 1$ (upper figures) and $S = 0.5$ (lower figures).

$S = 0$ case, see (A.3), and (b) position M (i.e., the start of the rectangular region which trails the nose) propagates backward ($h_M = h_N > 0.5$ for all $H \geqslant 1$).

Consider $0 < S < 1$. The manipulation of (3.1) suggests the transformation

$$A = (1 - S)\sqrt{\frac{H}{S}}, \quad \xi = \xi(h) = \left[1 + A\left(\frac{H}{S}\right)^{1/2}\frac{1}{h}\right]^{1/2}, \tag{3.14}$$

and, after some algebra, we obtain

$$\Upsilon(h) = Af(\xi) \tag{3.15}$$

where

$$f(\xi) = \frac{\xi}{\xi^2 - 1} + \frac{1}{2}\ln\frac{\xi + 1}{\xi - 1}. \tag{3.16}$$

Substitution in (3.8)–(3.9) gives, for the characteristic domain LOM,

$$u = u(\xi) = A\big[f(\xi_L) - f(\xi)\big], \quad \frac{x}{t} = A\left[f(\xi_L) - f(\xi) - \frac{\xi}{\xi^2 - 1}\right] \quad (\xi_L \leqslant \xi \leqslant \xi_M), \tag{3.17}$$

where $\xi_L = \xi(1)$ and $\xi_M = \xi(h_N)$ (recall that $h_M = h_N$).

The value of h_N is provided by (3.10) and (2.18)

$$u_N = A\big[f(\xi_L) - f(\xi_N)\big] = Fr(h_N)h_N^{1/2} \times \left[1 - S\left(1 - \frac{1}{2}\frac{h_N}{H}\right)\right]^{1/2}, \tag{3.18}$$

and the results are displayed in Fig. 3. Again, a similar equation and results for h_N and u_N have been obtained by UH without solving the details of the region behind the nose.

The analytical predictions for the dam-break propagation for the case $S = 0.5$, $H = 3$ and comparison with the numerical solution of the SW equations are shown in Fig. 4. The agreement between the analytical and numerical solutions is perfect before the backward-moving wave L reaches the wall at $x = -1$. Afterwards, the forward-moving reflected wave, not captured by the present analytical solution, influences the interface near the wall. Again, point M propagates backward, like in the previous $S = 1$ case. Actually, for the $S = 1$ case $u_M < 0$ for all H, but for smaller S and large H, u_M may be positive. (We emphasize that the details given here are for the present Fr correlation.)

The foregoing results are encouraging because they display acceptable physical behaviour and trends of the dam-break stage of the gravity current, and are a quite straightforward extension of the homogeneous $S = 0$ case. It is of course important to strengthen the agreement with the true physical system. The experiments of [5] confirm the existence of motion with constant u_N during the initial stage of propagation, in accordance with the dam-break prediction, and the quantitative agreement of the theoretical u_N with these experiments has been assessed by UH. However, these experiments were not concerned directly with the initial dam-break behaviour. We use here "numerical experiments" to gain some insight into this issue. The simulation is performed via a finite-difference solution of the Navier–Stokes equations in two dimensions, formulated for the variables (u, w, p, ϕ), where ϕ is the reduced density function whose value is 1 in the current, and 0 at the top and S at the bottom of the ambient, respectively. No slip conditions are applied on the bottom, back and front boundaries of the container (tank), while the top boundary of the container is treated as a frictionless lid. This makes the simulation compatible with real rectangular open-tank laboratory systems. Forward-time and central-space discretizations are used in the continuity and momentum equations, and MacCormack's forward–backward explicit method is used for the density function convection equation to prevent spurious oscillations at the interface. More details about this code are described in UH. The numerical code has been used and verified in various problems of gravity currents and stratified flows (UM, [18,19]). By numerical tests and analysis we estimate that the numerical errors of the velocity field in the currents simulated here are less than 1%. We consider currents with $H = 3$, $S = 1$ and 0.5 whose SW results were discussed above. Corresponding results for the non-stratified $S = 0$ case are also given in Appendix A. In the simulations $\epsilon = 0.05$ and $Re = Uh_0/\nu = 8333$; the initial aspect ratio $x_0/h_0 = 4$, the horizontal length of the channel is 3.5, the grid is 200×200, and the time-step 0.001. This configuration is compatible with laboratory salt-water experiments in an open tank of about 30 cm × 150 cm (height × length) and at least 10 cm width.

Density contour plots at $t = 1$ and 1.5 are displayed in Fig. 5 (see also Fig. 12 in Appendix A). The Navier–Stokes simulations display a fair global agreement with the SW predictions. The dense fluid displays, after a quick adjustment motion, flow-field domains that can be identified with the regions of Fig. 2: MN following the head, LM with inclined interface, and unperturbed LW. The nose is a prominent discontinuity and propagates with velocity close to the predicted u_N. Indeed, the SW predictions are that at $t = 1.5$ the nose is at $x_N = 0.33$ and 0.71 for $S = 1$ and 0.5, respectively (see Fig. 4), which is in very good agreement with the position of the nose obtained in the Navier–Stokes simulations, Fig. 5. The head is higher and slower for the larger S case. The depression wave of the interface reaches the wall $x = -1$ at (approximately) the time predicted by the SW theory. However, the shape on the interface in domain LM differs from the SW predictions, perhaps as a result of the strong shear about the interface in the real flow. We emphasize that this discrepancy between the SW and Navier–Stokes results is also observed in the homogeneous $S = 0$ case.

Contour lines of the simulated $u(x, z, t)$ fields at $t = 1$ and 2 are shown in Fig. 6 (see also Fig. 13 in Appendix A). The comparison with the SW results (see Fig. 4) indicates fair agreement in the WM (practically, $x < 0$) domain; however, in the domain of fluid that trails the nose u displays some fluctuations about the constant (average) value predicted by the SW theory. This is not surprising, since the nose of a real gravity current is known to be a very complicated flow-field (Simpson and Britter [20], Härtel et al. [21]), and the SW theory lumps this behaviour in an idealized jump condition. We emphasize that this deviation from the SW theory is not a result of the stratification; in this respect, the non-stratified $S = 0$ simulations are not different from the $S = 1$ and 0.5 cases.

Fig. 5 shows that, as expected, the release of the current in the stratified ambient produces significant perturbations in the ambient density field, in particular above the head. This effect is omitted in the present one-layer SW formulation. The leading internal wave velocity is, see (2.20), 0.55 and 0.40 for the $S = 1$ and 0.5 cases presented here, while the corresponding u_N is 0.22 and 0.47. Therefore, the $S = 1$ case is "subcritical" and the second one "supercritical". In the first case, the elevation of the density contours from the initial position is more pronounced, but in the time interval displayed here this difference is not of real significance to the motion of the current. In both cases, the major deviation of the density contours from the initial level is above the nose – then this line returns to its initial height, approximately, at $x = 0$. The SW theory predicts that $h = h_N = \text{const}$

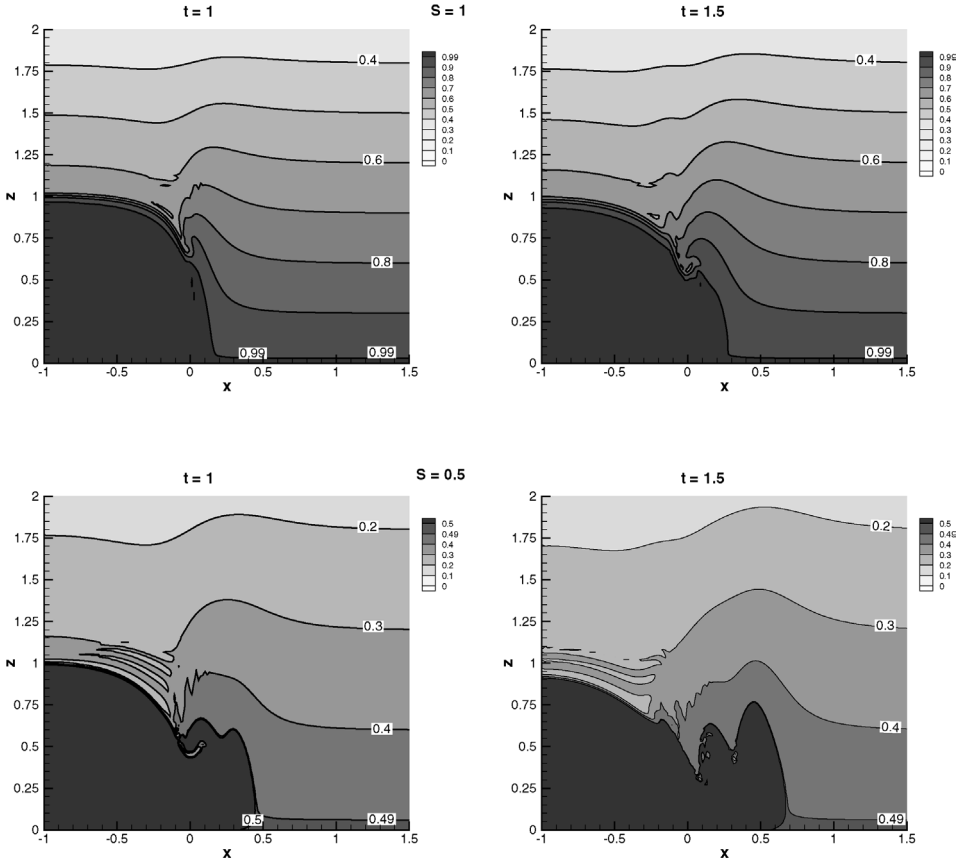

Fig. 5. Navier–Stokes numerical results: contours of the density function $\phi = [\rho(x, z, t) - \rho_o]/(\epsilon\rho_o)$ at two times, for $S = 1$ (upper figures) and 0.5 (lower figures). In both cases $H = 3$. (Recall that at $t = 0$: in the dense fluid $\phi = 1$, while in the ambient $\phi = 0$ at the top and $\phi = S$ at the bottom.)

in this region ($0 < x < h_N$, approximately) and that the density of the ambient above it is the unperturbed one at this level. This seems to be a fair approximation, on the average above the head, for the time periods considered here. Also, we observe that the perturbation of density in front of the current head is small at these times. Consequently, the global pressure head driving force balance calculated from the unperturbed hydrostatic balance can be expected to remain validity in spite of the local density waves. This vindicates the use of (2.10) and (2.16) during the initial period of propagation for both subcritical and supercritical u_N.

Indeed, as mentioned in Section 2.3, the waves interact with the head when its speed is "subcritical", but the first significant effect occurs after a distance of propagation of at least $4\pi(H/S)^{1/2}(h_0/x_0)u_N \approx 1.2$ in the example, and the time to this occurrence is 5.5 at least. The time of formation and propagation of this interaction effect exceed the pertinent dam-break time interval, and we therefore expect that these waves do not affect the presently investigated dam-break motion. We think that the present results indicate that in many interesting configurations the waves can be added to the flow-field of this model at a later stage of propagation, but this is a quite complicated topic that we leave for future investigation.

3.2. Non-linear stratification

In practical circumstances the density of the ambient, $\rho_a = \rho_o[1 + \epsilon S\sigma(z)]$, is not necessarily a linear function of z. For example, sampling the fluid in an experimental tank after the double-bucket filling procedure, often reveals some deviations from the idealized linear $\sigma(z)$. Diffusion is able to eventually linearize the profile, but this requires the postponement of the experiment for several hours, typically. The present formulation allows the incorporation of a non-linear $\sigma(z)$, as follows. The analytical results (3.4)–(3.10) remain valid. However, the integrals $\Lambda(h_N)$ and $\Upsilon(h)$, see (2.17) and (3.1), require, in general, a numerical evaluation for a non-linear $\sigma(z)$. This is a straightforward task (including, of course, cases of measured profiles).

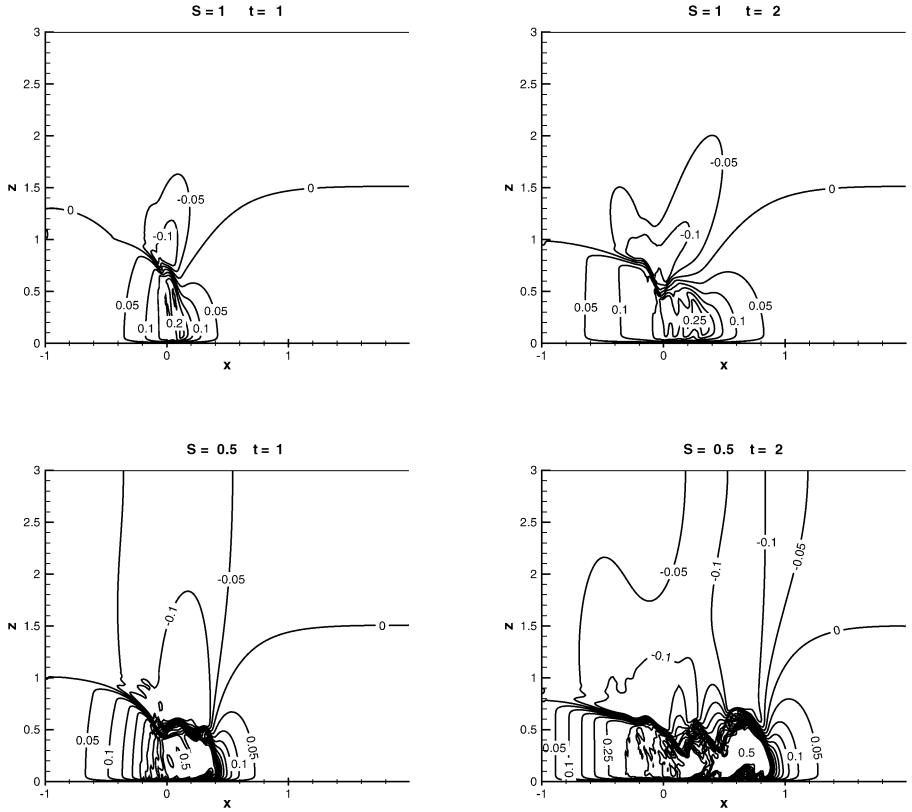

Fig. 6. Navier–Stokes numerical results: contours of the horizontal velocity $u(x,z)$ at two times, for $S=1$ (upper figures) and 0.5 (lower figures). In both cases $H=3$.

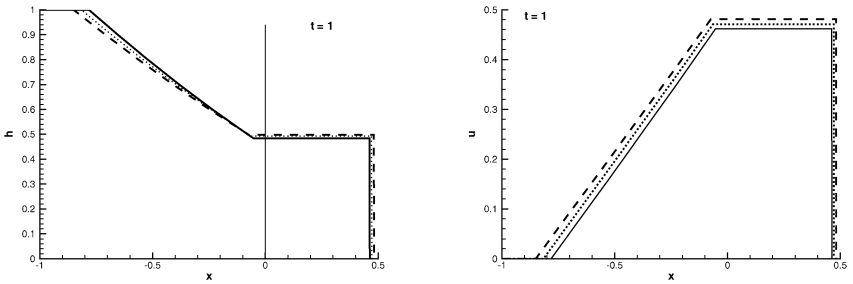

Fig. 7. Analytical results of $h(x)$ and $u(x)$ at $t=1$, for $S=0.5$, $H=3$, different stratifications: (a) $\sigma(z)=1-(z/H)+0.5(z/H)[1-(z/H)]$, full line; (b) $\sigma(z)=1-(z/H)-0.5(z/H)[1-(z/H)]$, dashed line; (c) linear $\sigma(z)=1-(z/H)$, dotted line.

Here we briefly illustrate the influence of this effect on the dam-break flow results. We consider, again, the case $S=0.5$, $H=3$. Now we incorporate in the analysis deviations about the linear stratification, namely, we produce solutions for the two density functions

$$\sigma(z)=\sigma_{\text{linear}}(z)\pm 0.5(z/H)\big[1-(z/H)\big].$$

The influence of the last term is shown in Fig. 7 via a comparison to the linear case. The decreased $\sigma(z)$ (i.e., when the minus sign in the previous equation is taken) produces larger u_N and $|u_L|$, and vice-versa. This could be anticipated: when the deviation is towards the homogeneous ambient, the flow tends to the homogeneous case results. For both the $\pm$ non-linear density deviations, the quantitative deviations of h and u results from the behaviour predicted for the linear stratification are relatively small. This is because the contributions of the tested non-linear terms to the integrals (2.17) and (3.1) turn out to be

small. This result is expected to be typical. Evidently, a more complex non-linear density profile can be easily accommodated by the present procedure if necessary in the interpretation of experimental and environmental data.

The non-linear stratification features may also be of interest in future studies on the stability of the flow.

3.3. Elliptical (or cylindrical) lock

The rectangular lock reservoir used in the foregoing investigation of the dam-break problem is a very special configuration. An interesting question is what changes and similarities in the resulting flow field are expected when the gravity current is released, again in a two-dimensional xz configuration, but from a lock (reservoir) of a different shape. To gain some insights we consider an elliptical (or cylindrical) reservoir, i.e. the initial condition

$$h(x, t = 0) = \chi(x) = (-x^2 - 2x)^{1/2} \quad (-1 \leqslant x \leqslant 0). \tag{3.19}$$

This shape may be relevant to atmospheric and oceanic currents generated by the collapse of a naturally produced (and hence more likely of a round shaped than rectangular initial contour) mixed region of stratified fluid. The initial velocity is zero. We consider the linearly stratified ambient.

A closed analytical solution by the method of characteristics like in the rectangular problem is not feasible. However, some simple useful approximations for the initial motion can be obtained. We attempt an expansion of u and of the displacement of the interface in powers of t (for $t \ll 1$). Substitution in the governing equations (2.13) yields the leading terms (for $t \ll 1$, $-1 \leqslant x < 0$)

$$u = (x + 1)\left[\frac{S}{H} + \frac{1 - S}{\chi(x)}\right]t, \tag{3.20}$$

$$h = \chi(x) - \frac{1}{2}\left[1 - S - \frac{S}{H}\frac{2(x + 1)^2 - 1}{\chi(x)}\right]t^2. \tag{3.21}$$

(The next terms are $O(t^3)$ for u and $O(t^4)$ for h, but the coefficients are cumbersome.) The (quite weak) singular behaviour of the time dependent terms as $x \to 0^-$ is relaxed by the development of a nose of increasing height h_N that propagates forwardly. The details cannot be obtained from this approximation, but continuity with (3.20) and characteristic balances indicate that $h_N \approx 0.5t$. The approximation (3.20), (3.21) points out the essential differences between the flow-fields after release from a rectangular and a cylindrical lock. In the former case, the perturbation propagates slowly from the nose into the reservoir, and a (shrinking) domain of unperturbed fluid ($h = 1$, $u = 0$) can be found for some time ($t \approx 1$) after release. In the latter case, the motion begins instantaneously in the entire body of dense fluid. The interface descends near the endwall $x = -1$ and rises in the frontal region, while u develops an increasing with x profile. The obvious reason for this behaviour is the fact that a significant horizontal pressure gradient exists in the stationary dense fluid in the elliptical lock (proportional to the initial $\mathrm{d}h/\mathrm{d}x$) while in the rectangular lock this effect is absent. The stratification of the ambient, represented by S, reduces the initial effect of the pressure gradient.

The finite-difference solution of the SW equations for this configuration by our code (developed for the classical rectangular lock) turned out to be a straightforward task. The numerical initial conditions for h were changed to values provided by (3.19) for the internal grid points, and a small non-zero h_N (typically 0.01) was taken at $x = x_N = 0$. The results were subjected to various convergence tests and we concluded that the numerical accuracy is similar to that of the classical rectangular case. Results for a configuration with $S = 0.5$ and $H = 3$ are presented in Figs. 8 and 9.

Fig. 8 depicts the behaviour of h and u for small t. We can see that approximate results capture well the features of the initial behaviour in the domain $-1 \leqslant x < 0$. The numerical SW results show that h_N increases quickly from zero (the value 0.3 is reached at $t = 0.6$). During the initial time the maximum of u in the dense fluid is attained at $x \approx 0$. Overall, the foregoing interpretation of the initial motion as a result of the pressure gradient is confirmed. The initial motion predicted by the inviscid SW model displays strong velocity gradients in the domain $0 < x < x_N$. This will certainly involve viscous smoothing, mixing and hindrance effects in a real fluid.

Fig. 9 illustrates the behaviour of the current at more advanced times, when some rather surprising features appear. While the rear part of the interface ($-1 \leqslant x < 0$) descends and flattens horizontally, h_N increases until it attains the value of a slumping rectangular counterpart, cf. Fig. 4, at $t \approx 2$. However, the c_+ characteristics that reach the nose are emanated by a domain of varying u and h, and therefore this value of h_N cannot be maintained. Indeed, afterwards h_N decreases, and a rectangular region of constant h (like that which trails the nose in the rectangular-lock case) does not develop. In Fig. 9(b) we see that the velocity of propagation, u_N, has a clear acceleration–deceleration behaviour, as opposed to the constant u_N which appears in the rectangular-lock case. However, the maximal velocity of the nose in the cylindrical-lock case is equal to u_N of the slumping rectangular-lock current. Again, a stage of constant u_N does not develop, but we note that for $1 < t < 3$ the values of u_N do not differ much from the maximum. Practically (i.e., for experimental verifications) the currents released

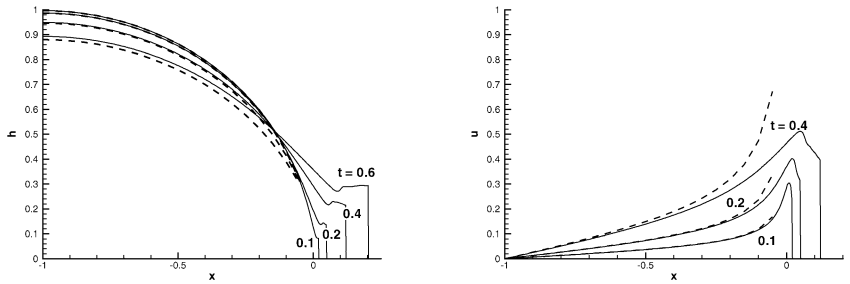

Fig. 8. Cylindrical-lock release for $S = 0.5$, $H = 3$, profiles of h and u as functions of x at various times. SW numerical results (solid line) and analytical approximations (dashed line).

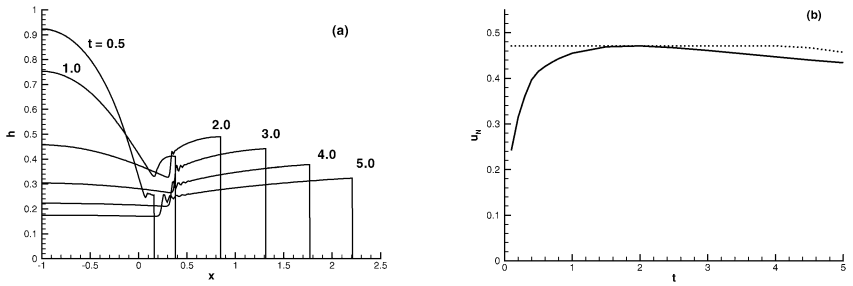

Fig. 9. Cylindrical-lock release for $S = 0.5$, $H = 3$, SW numerical results. (a) Profiles of h as a function of x at various times; (b) u_N as a function of time (solid line), and also shown the values for the rectangular-lock counterpart (dotted line).

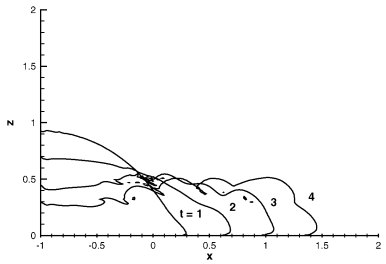

Fig. 10. Cylindrical-lock release for $S = 0.5$, $H = 3$, Navier–Stokes numerical contours of the current at various times, for $h_0/x_0 = 1$.

from cylindrical and rectangular locks are expected to display very similar distances of propagation (the values of x_N at $t = 5$ are 2.21 and 2.35, respectively), although the volume of the former current is by about 21% smaller. The main difference would be a more pronounced acceleration–deceleration pattern, with a sharp maximum, for the cylindrical lock.

Navier–Stokes simulated profiles of the current, for $S = 0.5$, $H = 3$, $h_0/x_0 = 1$ and $Re = Uh_0/\nu = 1.7 \times 10^4$, are presented in Fig. 10. These results corroborate the global insights provided by the SW analysis. The SW model captures well the tendency of the cylinder to first flatten to an approximately rectangular shape, then of the bulk in $x < 0$ to become thinner than the front. The development of the flow in the NS simulations is slightly slower than in the SW prediction. The mean velocity of propagation in the time interval 1 to 4 is about 0.40 in the NS simulation, about 10% less than the SW prediction. This can be attributed to the viscous effects which are expected to play a significant role during the initial stage, when the head is thin and the velocity is small. On the other hand, it is encouraging to note that the theory provides useful results even for the $h_0/x_0 = 1$ cases (although, formally, the SW results are restricted to $h_0/x_0 \ll 1$).

4. Concluding remarks

The dam-break problem solution for the release of a gravity current has been extended to the case of a stratified ambient. We showed that the one-layer shallow-water (SW) formulation of UH, extended here to non-linear stratifications, is amenable to analytical solutions (by the method of characteristics). For linear stratification closed formulas were obtained, and in the

more general case some simple numerical quadratures may be necessary for expressing the height of the interface, h, and the velocity, u, as functions of x and t. The SW equations were also solved by a finite-difference Lax–Wendroff scheme, and comparisons show excellent agreement with the analytical predictions. In the limit of zero stratification ($S = 0$) the classical one-layer dam-break solution is identically recovered.

Qualitatively, the stratified and non-stratified cases are similar: after the removal of the gate at $x = 0$, three regions form instantaneously: a shrinking domain of unperturbed fluid on one side ($x < 0$), a domain of constant height h_N and velocity u_N on the other side ($x > 0$), and in between a matching domain of continuously varying h and u. The details depend on the magnitude and shape of stratification, S and $\sigma(z)$. In particular, the rate of propagation of the current and shrinking of the unperturbed region are reduced when S increases. For linear stratification in which the density of the ambient at the base is equal to that of the current ($S = 1$), h displays a linear dependency on x in the matching region, quite different from the parabolic profile in the classical $S = 0$ case. No internal discontinuities (shocks) develop.

The present results provide (a) insights into the initial behaviour of the current and influence of the main dimensionless parameters, (b) a convenient tool for the validation of numerical codes, and (c) a reliable starting flow-field for the investigation of additional effects, such as waves, stability and mixing. The effect of non-linear stratification is of interest in the interpretation of experimental and environmental data for which deviations from the linear stratification are common. Moreover, the present SW results provide the link between the slumping motion of the nose predicted by UH and the motion in the entire bulk of dense fluid. The good agreement between the predicted u_N and the experiments of Maxworthy et al. [5] reported by UH strengthen the physical relevance of the theoretical analysis.

The classical dam-break configuration considers a rectangular reservoir of dense fluid. We contrasted it with the expected behaviour of release from a cylindrical lock. In the second case a pronounced acceleration–deceleration velocity of propagation is expected (in the time interval for which the first case displays a constant velocity). The maximal velocity of propagation, and the effect of stratification, are the same for both cases.

Additional support to the SW insights has been provided in this work by numerical solutions of the full Navier–Stokes equations. Overall, the essentials of the motion are captured well by the averaged simplified SW model, and, in our opinion, the performances of the model are the same for $S = 0$ and $0 < S \leqslant 1$ during the dam-break time interval, at least. However, there are some features that require further attention. Experiment and the Navier–Stokes solution indicate that the release of the current produces significant perturbations in the ambient density field, in particular above the head. The propagation of these stratification waves created by the dam-break is an interesting topic for future investigation, perhaps along the lines of Schooley and Hughes [22] and of Baines [11] (regarding the current as an obstacle at the bottom of a moving stratified fluid); but the coupling between the current and the waves produces a formidable analytical problem. There is experimental and numerical evidence (see [5,9]) that these waves may interact eventually with the head of the current and hinder its propagation. However, in the present investigation of the dam-break initial stage of motion no significant difference between subcritical and supercritical currents was detected.

The present SW formulation uses the one-layer model, which discards the motion of the ambient fluid and thus prevents the investigation of coupling effects between the upper and lower layers of fluid. In non-stratified circumstances the influence of the upper layer is very significant for configurations with $H < 2$, as pointed out by Rottman and Simpson [12], Klemp et al. [4] and Ungarish and Zemach [13]. These studies show that the influence of the upper layer is quite accurately reproduced by the two-layer SW model. When $H < 2$, the most pronounced feature during the dam-break stage is the formation of a backward-moving discontinuity (jump) of h at position L (which is subsequently reflected at $x = -1$ as a forward-moving bore). In addition, when H approaches 1, the slumping distance of propagation with constant u_N is significantly prolonged, and in some circumstances the maximum velocity of the c_+ characteristic imposes choking limitations on the propagation of the nose. The one-layer model misses these effects for $H < 2$, but predicts fairly well the initial velocity of propagation. For large H ($\geqslant 3$, say) the differences between the two and one-layer models are rather academic. For the stratified case the corresponding effects and deficiencies of the one-layer model for $H < 2$ (say) are not known. The big theoretical challenge here is the formulation of a clear-cut two-layer SW model. In the homogeneous ambient it makes sense to represent the motion in the upper layer by a z-independent vertical velocity $u_2(x,t) = -u(x,t)h(x,t)/[H - h(x,t)]$. The straightforward extension of this approximation to the stratified ambient is not expected to be valid because of the resistance to horizontal displacements and formation of waves and critical layers, see [11]. In any case, the one-layer model remains relevant in the investigation of the dam-break problem because it is amenable to analytical solutions which provide useful insights and guidelines.

These topics are left for future work. The precise formulation of the nose condition in a stratified ambient is also a topic that needs additional investigation in analytical, experimental and numerical directions. The condition used in this work can be replaced with other correlations when available. This allows the practical verification of new suggestions, and also the improvement of the present model.

The release of a gravity current from a cylindrical container into a stratified ambient is the axisymmetric counterpart of the foregoing investigation. This problem is also of interest, but not amenable to simple analytical solutions because of additional

curvature terms in the equations of motion. On the other hand, the Lax–Wendroff solver can be extended to this geometry. Some typical results are given in Appendix B.

Acknowledgements

Thanks to Prof. H.E. Huppert for stimulating discussions and Mrs. T. Zemach for useful comments. The research was supported by the Fund for Promotion of Research at the Technion.

Appendix A. Non-stratified $S = 0$ results

In this case (3.1) gives

$$\Upsilon(h) = 2\sqrt{h} \tag{A.1}$$

and hence in the characteristic MON domain, according to (3.8), (3.9),

$$u = 2(1-\sqrt{h}), \quad \text{on } \frac{x}{t} = 2 - 3\sqrt{h} \quad (h_N \leqslant h \leqslant 1). \tag{A.2}$$

This can be reformulated as

$$h = \frac{1}{9}\left(2 - \frac{x}{t}\right)^2, \quad u = \frac{2}{3}\left(1 + \frac{x}{t}\right), \quad -1 \leqslant \frac{x}{t} \leqslant 2 - 3\sqrt{h_N}. \tag{A.3}$$

In Saint-Venant's solution of the water-air dam break the nose condition is simply $h_N = 0$.

For the gravity current that propagates into a fluid of slightly different density, the value of h_N is provided by (3.10)

$$2(1-\sqrt{h_N}) = Fr(h_N)\sqrt{h_N}. \tag{A.4}$$

Results of the SW formulation are presented in Fig. 11. The backward-moving expansion wave reaches the wall at $t = 1$, which explains the discrepancy between the present analytical and Lax–Wendroff solution at later times.

Results of the Navier–Stokes solution (for details see Section 3.1) are presented in Figs. 12 and 13.

Appendix B. Axisymmetric configuration

Consider an axisymmetric cylindrical configuration similar to that of Fig. 1. The axis of symmetry, z, replaces the wall. Let r be the radial coordinate. The radius of the lock cylinder, r_0, is used to replace x_0 in the scaling (2.11), (2.12). (Roughly, r replaces $x + 1$ in previous notation.)

The governing SW equations are given by the system (2.13) with the modifications: (a) the x derivatives changed to r derivatives, and (b) the RHS of the continuity equation is $-uh/r$. The characteristic velocities are not affected, but that curvature term contributes $-a(h)uh\,\mathrm{d}t/r$ to the RHS of the characteristic balance (2.15), where $a(h)$ is the coefficient of $\mathrm{d}h$ in (2.15). The previous analytical solutions of the SW equations could not be extended to this case, but the numerical Lax–Wendroff scheme was modified to incorporate the additional terms. Results are presented in Fig. 14 for the same parameters as Fig. 4. At short time intervals after release the rectangular and axisymmetric dam-break flows are very similar, but eventually the curvature terms introduce significant differences.

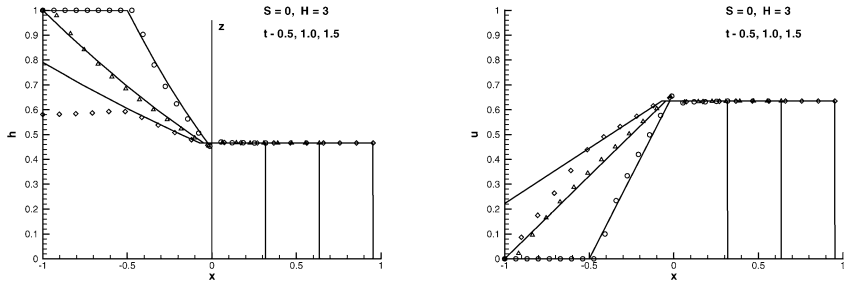

Fig. 11. Analytical (lines) and SW numerical (symbols) results, of $h(x)$ and $u(x)$ at $t = 0.5, 1.0, 1.5$, for non-stratified $S = 0$ case.

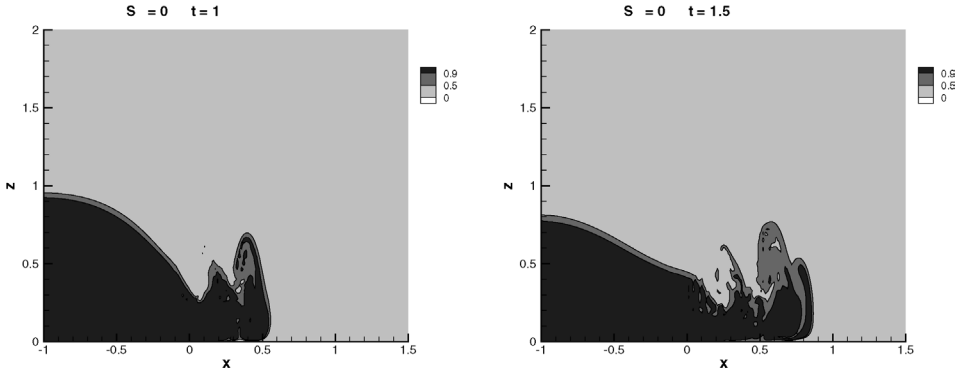

Fig. 12. Navier–Stokes numerical results: contours of the density function at two times, for $S = 0$ and $H = 3$.

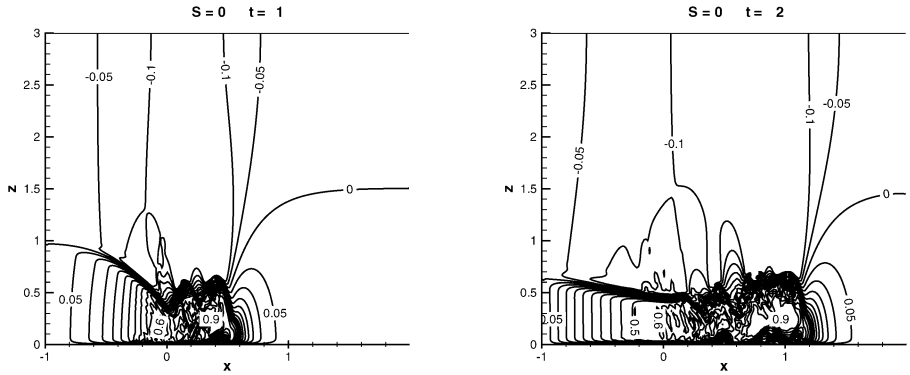

Fig. 13. Navier–Stokes numerical results: contours of the horizontal velocity $u(x, z)$ at two times, for $S = 0$ and $H = 3$.

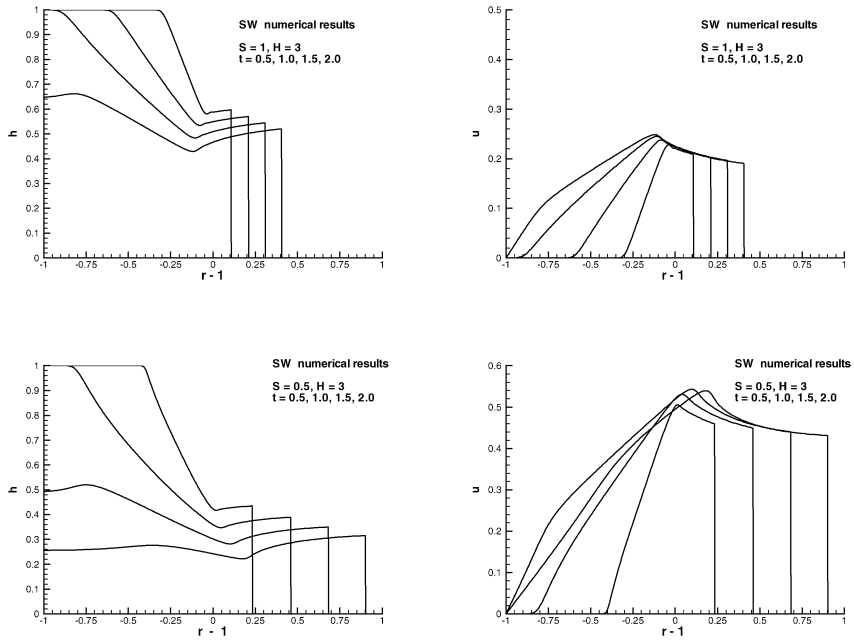

Fig. 14. Linear stratification, axisymmetric case, SW numerical results of $h(r)$ and $u(r)$ at various times, for $H = 3$, $S = 1$ (upper) and $S = 0.5$ (lower).

References

[1] J. Billingham, A.C. King, Wave Motion, Cambridge University Press, 2000.
[2] J.E. Simpson, Gravity Currents in the Environment and the Laboratory, Cambridge University Press, 1997.
[3] H.E. Huppert, Geological fluid mechanics, in: G.K. Batchelor, H.K. Moffatt, M.G. Worster (Eds.), Perspectives in Fluid Dynamics: A Collective Introduction to Current Research, Cambridge University Press, 2000, pp. 447–506.
[4] J.B. Klemp, R. Rotunno, W.C. Skamarock, On the dynamics of gravity currents in a channel, J. Fluid Mech. 269 (1994) 169–198.
[5] T. Maxworthy, J. Leilich, J.E. Simpson, E.H. Meiburg, The propagation of gravity currents in a linearly stratified fluid, J. Fluid Mech. 453 (2002) 371–394.
[6] M. Ungarish, H.E. Huppert, On gravity currents propagating at the base of a stratified ambient, J. Fluid Mech. 458 (2002) 283–301 (referred to as UH).
[7] T.B. Benjamin, Gravity currents and related phenomena, J. Fluid Mech. 31 (1968) 209–248.
[8] H.E. Huppert, J.E. Simpson, The slumping of gravity currents, J. Fluid Mech. 99 (1980) 785–799.
[9] M. Ungarish, Intrusive gravity currents in a stratified ambient – shallow-water theory and numerical results, J. Fluid Mech., 2005, in press.
[10] M. Ungarish, H.E. Huppert, On gravity currents propagating at the base of a stratified ambient: effects of geometrical constraints and rotation, J. Fluid Mech. 521 (2004) 69–104.
[11] P.G. Baines, Topographic Effects in Stratified Flows, Cambridge University Press, 1995.
[12] J. Rottman, J. Simpson, Gravity currents produced by instantaneous release of a heavy fluid in a rectangular channel, J. Fluid Mech. 135 (1983) 95–110.
[13] M. Ungarish, T. Zemach, On the slumping of high Reynolds number gravity currents in two-dimensional and axisymmetric configurations, Eur. J. Mech. B Fluids 24 (2005) 71–90.
[14] K.W. Morton, D.F. Mayers, Numerical Solutions of Partial Differential Equations, Cambridge University Press, 1994.
[15] W.H. Press, S.A. Teukolski, W.T. Vetterling, B.P. Flannery, Numerical Recipes in Fortran, Cambridge University Press, 1992.
[16] R.T. Bonnecaze, H.E. Huppert, J.R. Lister, Particle-driven gravity currents, J. Fluid Mech. 250 (1993) 339–369.
[17] M. Ungarish, H.E. Huppert, The effects of rotation on axisymmetric particle-driven gravity currents, J. Fluid Mech. 362 (1998) 17–51.
[18] M. Ungarish, T. Zemach, On axisymmetric rotating gravity currents: two-layer shallow-water and numerical solutions, J. Fluid Mech. 481 (2003) 37–66.
[19] J.B. Flor, M. Ungarish, J.W.M. Bush, Spin-up from rest in a stratified fluid: boundary flows, J. Fluid Mech. 472 (2002) 51–82.
[20] J. Simpson, R.E. Britter, The dynamics of the head of a gravity current advancing over a horizontal surface, J. Fluid Mech. 94 (1979) 477–495.
[21] C. Härtel, E. Meiburg, F. Necker, Analysis and direct numerical simulation of the flow at a gravity current head. Part 1. Flow topology and front speed, J. Fluid Mech. 818 (2000) 189–212.
[22] A.H. Schooley, B.A. Hughes, An experimental and theoretical study of internal waves generated by the collapse of a two-dimensional mixed region in a density gradient, J. Fluid Mech. 51 (1972) 159–175.